Pergamon

Acta mater. 49 (2001) 1463–1470

Acta MATERIALIA

www.elsevier.com/locate/actamat

REACTION SYNTHESIS OF TiB_2–TiC COMPOSITES WITH ENHANCED TOUGHNESS

G. WEN[1, 2], S. B. LI[1], B. S. ZHANG[1] and Z. X. GUO[2]†

[1]School of Materials, Harbin Institute of Technology, Harbin 150006, PR China and [2]Department of Materials, Queen Mary, University of London, London E1 4NS, UK

(Received 30 January 2000; received in revised form 3 January 2001; accepted 3 January 2001)

Abstract—*In situ* toughened TiB_2–TiC_x composites were fabricated using reaction synthesis of B_4C and Ti powders at high temperatures. The resulting materials possessed very high relative densities and well developed TiB_2 plate-like grains, leading to a rather high fracture toughness, up to 12.2 MPa•$m^{1/2}$. The microstructure was examined by means of XRD, SEM, TEM and EDAX. The reaction products mainly consisted of TiB_2 and TiC_x. No other phases, e.g. Ti_3B_4, TiB, Ti_2B_5 and free Ti, were observed regardless of whether the starting composition was Ti:B_4C = 3:1 or 4.8:1, and whether the sintering temperature was 1700 or 1800°C. The microstructural morphology is characterised by TiB_2 plate-like grains distributed uniformly in the TiC_x matrix. Some inclusions and defects were found in TiB_2 grains. The very high reaction temperature was believed to be responsible for the formation of plate-like grains, which, in turn, is responsible for the much improved mechanical properties. The main toughening mechanisms were likely to be crack deflection, platelet pull-out and the micro-fracture of TiB_2 grains.

Keywords: Reaction synthesis; Composites; High temperature

1. INTRODUCTION

Carbide and boride ceramics possess many desirable properties, such as high hardness, low density, high melting temperature, and high corrosion resistance. Particularly, these materials are characterised by a high electrical conductivity and hence readily machinable by means of electric discharge. These are the promising candidates for cutting tools, wear proof parts, amour, and new type of electrodes. However, each of the monolithic materials, as with other ceramics, possesses a low toughness, which hinders their applications [1–3].

The most promising approach to toughening these two ceramics may be to form a composite by the addition of other ceramic particles, whereas other known routes, such as transformation toughening and fibre toughening, are difficult to employ in such a case because of the very high sintering temperature involved. TiB_2–B_4C and TiB_2–TiC–SiC composites are good model systems that have been explored in the past [4–7].

Recently, a relatively new method, so-called *in situ* reaction toughening, has been used to fabricate composites with TiB_2 as a reinforcement, which relies on the reactivity of B_4C with Ti-based materials (metal, carbide and nitride). Moriyama and Aoki [8] have produced TiB_2–TiN_xC_y composites by this method from B_4C and TiN powder mixtures. Sasaki *et al*. [9] have fabricated B_4C–TiB_2 composites from the reaction of B_4C and TiC. Hofmann [10] has obtained B_4C–TiB_2–W_2B_5 composites by the reaction of B_4C and TiC–WC–Co. Barsoum and Houng [11] have prepared TiB_2–TiC composites by hot pressing of B_4C and Ti powder mixtures at 1600°C, where relatively high mechanical properties are obtained with a bending strength of 590 MPa and a fracture toughness of 5.6 MPa•$m^{1/2}$. A so-called TPPP (Transient Plastic Phase Processing) technique has been developed, and the composites can be plastically formed into complex shapes during hot pressing. Similar TiB_2–TiC composites have been fabricated by pressure-assisted thermal explosion and reactive hot pressing, respectively, from the starting powder composition of Ti:B_4C = 3:1, where, a lower processing temperature of 1000°C and a higher pressure of 150 MPa were used. The resulting bending strength and fracture toughness reach 190–210 MPa and 5.9–6.6 MPa•$m^{1/2}$, respectively [12].

A similar research on the B_4C–Zr system has been carried out by Johnson and co-workers [13–15], where the Zr liquid is allowed to infiltrate a B_4C pow-

† To whom all correspondence should be addressed. Tel: +44-020-7882-5569; Fax: +44-020-8981-9804.
E-mail address: x.guo@qmw.ac.uk (Z.X. Guo)

1359-6454/01/$20.00
PII: S1359-6454(01)00034-9

der bed and the reaction between them takes place at relatively high temperatures. The resulting materials consist of ZrB_2, ZrC_x and free Zirconium, in which ZrB_2 is of a platelet morphology leading to a very high toughness, i.e. from 12 MPa•$m^{1/2}$ for very little free Zr content to 20 MPa•$m^{1/2}$ for 30% free Zr [13–15]. However, the formation of this microstructure needs a rather long time for the relevant diffusion and reaction to take place and to finish, particularly for the removal of the free Zr when high refractory materials are required.

Clearly, there is a large scope for improvement in terms of microstructure and properties of the B_4C–Ti system, in comparison with the B_4C–Zr system. The main reason why the mechanical properties of the B_4C–Ti system is not as good as that of the B_4C–Zr system is discussed in this study. The simplicity of hot pressing and the advantages of transient liquid sintering were here combined for the preparation of TiB_2–TiC composites with improved microstructure and mechanical properties. The microstructure of the resulting materials was investigated by XRD, SEM and TEM analyses. The mechanical properties were evaluated by 3-point bending and single edge notched beam testing.

2. EXPERIMENTAL PROCEDURES

2.1. Material preparation

Commercially available B_4C and Ti powders were used as starting materials. The B_4C powder is angular with a particle size of 2–5 μm and ~5% free carbon as the main impurity. The Ti powder is spherical with a particle size of 4–10 μm and small traces of H and O as impurities. Two molar ratios (Ti to B_4C) of 3:1 and 4.8:1 were chosen as the starting compositions. Hereafter the resulting materials are referred to as 3Ti–B_4C and 4.8Ti–B_4C, respectively. The 3:1 molar ratio is the same as used in [11, 12], which was selected here to evaluate the effect of a higher sintering temperature on the microstructure and properties of the materials in comparison with the early works [11, 12]. The 4.8:1 ratio was chosen with the aim of modifying the reaction products.

The powders were mixed by dry ball milling for 12 h under ~150 rpm in a plastic bottle with WC balls as the medium. The powder mixture was hot pressed at 1800°C under 35 MPa for 60 min. In order to investigate the effect of sintering temperature, 4.8Ti–B_4C samples were also sintered at 1700°C, under 35 MPa for 60 min. The starting composition and sintering parameters are summarised in Table 1. Hot pressing was conducted in a vacuum hot press at 10^{-4} torr between graphite dies without inner coating. The resulting plates were about Φ60×6 mm^2 in size. These were often firmly bonded to the inner wall of the graphite die, due to die/sample reaction. Some small beads were found adhered to the surface of the die, which may be related to the flow of Ti from the powder compact. A layer of about 1 mm was removed from both surfaces before the specimens were subjected to microstructure or property characterisation.

2.2. Characterisation

XRD was used to identify the reaction products. TEM was used for more detailed microstructural analysis. Both polished and fractured surfaces were examined by SEM. The phases were also characterised by means of EDAX with an ECON detector. Porosities in the sintered samples were determined by standard densitometry.

The samples were cut to various sizes for mechanical property tests with an electrical discharge saw. The bending strength (σ_b) was evaluated by three point bending using an Instron instrument with a specimen size of 3×4×36 mm^3, and a crosshead speed of 0.5 mm/min. The tensile edges were bevelled and the tensile surface was polished with 1 μm diamond paste. With the same equipment as used for bending test, fracture toughness (K_{IC}) was studied by the single edge notched beam (SENB) method on notched specimens of 2×4×20 mm^3, with a crosshead speed of 0.05 mm/min. The values are listed in Table 1, where each data point presents an average of 5–6 measured values.

3. RESULTS AND DISCUSSION

3.1. Reaction products

In order to identify the reaction mechanisms, the reaction products of the sintered samples were first subjected to XRD analysis. The results are shown in Fig. 1. It is noted that the phases of all the specimens are TiB_2 and TiC_x (x is the stoichiometry of the TiC_x compound and is not accurately determined in the present study). There seemed to be no other phases, such as TiB, Ti_3B_4, Ti_2B_5 and free Ti, although the original composition and sintering temperature varied.

The reaction products are identical to those reported by Barsoum and Houng [11] for a 3Ti–B_4C compact hot pressed at 1600°C, indicating that the higher temperature has no effect on the species of the reaction products for the 3:1 composition. The reaction mechanism is likely to involve:

$$3Ti + B_4C \rightarrow 2/3TiB + 2/3Ti_2B_5 + TiC \quad (1)$$

and then

$$2/3TiB + 2/3Ti_2B_5 \rightarrow 2TiB_2 \quad (2)$$

and, hence, the net reaction is

$$3Ti + B_4C \rightarrow 2TiB_2 + TiC \quad (3)$$

However, the resulting phases of the 4.8Ti–B_4C

Table 1. Composition of starting materials, sintering parameters and properties of the composites

Materials	Composition of starting materials Ti/B_4C (molar ratio)	Sintering parameters			Mechanical properties	
		Temp. (°C)	Press. (MPa)	Time (min)	σ_b (MPa)	K_{IC} (MPa•$m^{1/2}$)
3Ti–B_4C	3	1800	35	60	453.9±13.8	8.44±0.94
4.8Ti–B_4C	4.8	1700	35	60	504.6±66.9	8.58±1.80
4.8Ti–B_4C	4.8	1800	35	60	680.4±113.2	12.20±1.26

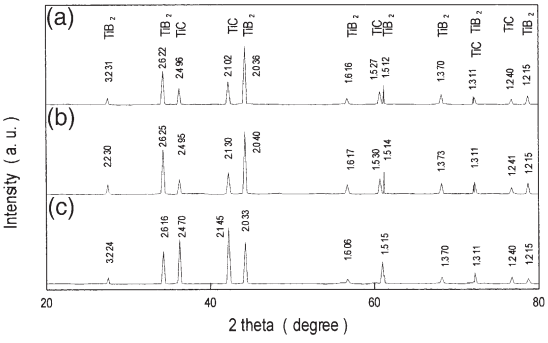

Fig. 1. XRD patterns of the materials: (a) 4.8Ti–B_4C hot pressed at 1700°C; (b) 4.8Ti–B_4C hot pressed at 1800°C; (c) 3Ti–B_4C hot pressed at 1800°C.

materials are different from those reported in Barsoum and Houng's study [11]. In the latter case, Ti_3B_4 was found for 4Ti–B_4C composition in addition to TiB_2 and TiC_x, when hot pressed at 1600°C, with the net reaction being:

$$4Ti + B_4C \rightarrow 0.33Ti_3B_4 + 1.67TiC_{0.6} + 1.33TiB_2 \quad (4)$$

In another investigation [16], Brodkin and Baroum reported that the final products were always TiB_2, $TiC_{0.65}$ and Ti_3B_4 for the composition of 4Ti–B_4C, whether it was hot pressed or heat-treated at 1600°C (for a long period of time, e.g. 16 h). For the composition of 5Ti–B_4C, TiB, Ti_3B_4 and a small level of TiB_2 were found after vacuum heat-treatment for 4 h at 1600°C, whereas TiB_2 disappeared after a long period of vacuum heat-treatment.

It is clear that for the 4.8Ti–B_4C composition in this study, the phases did not evolve according to the route suggested by Baroum *et al.* [11]. Two reasons may be attributed to this difference. One is the purity of the starting materials. Brodkin and Barsoum [16] pointed out that the nucleation and growth of Ti_3B_4 are sensitive to the impurity content, and Ti_3B_4 exists only when a high-purity Ti and a highly reducing atmosphere are employed. Ti used in this study is commercial powder, with a relatively high level of impurity, which is not favourable for the formation of Ti_3B_4. Another reason may be associated with the peritectic reaction of Ti_3B_4, which is related to the sintering temperature, or the actual temperature in the materials. The binary Ti–B diagram (see Fig. 2) shows the presence of a peritectic reaction at 2200°C [17]. The adiabatic temperature of the reaction (4) is calculated to be about 4020°C, where the preheating temperature (i.e. hot pressing temperature) is 1800°C; it is assumed that the reaction heat is fully used to increase the temperature of the products. Such a high temperature is sufficient to result in further transformation of Ti_3B_4 into TiB_2 and a liquid. Therefore even if it is produced via reaction (4), Ti_3B_4 would not be present in the final structure.

Such a high reaction temperature probably also explains why there is no free Ti in the present samples. According to the products examined by XRD, the overall reaction for the 4.8Ti–B_4C material may be described as follows:

$$4.8Ti + B_4C \rightarrow 2TiC_{0.5} + 2TiB_2 + 0.8Ti \quad (5)$$

Free Ti should have been present in the final material as indicated by reaction (5). However, flow of liquid Ti or vaporisation of Ti and the graphite die would take place at such high temperatures. Both the escaping of Ti and the ingress of carbon into the sample consumed free Ti in the system. The existence of the beads on the die surface lends support to this explanation.

This strong exothermal reaction is the predominant characteristic of this system, which influenced not only the species of the products but also the

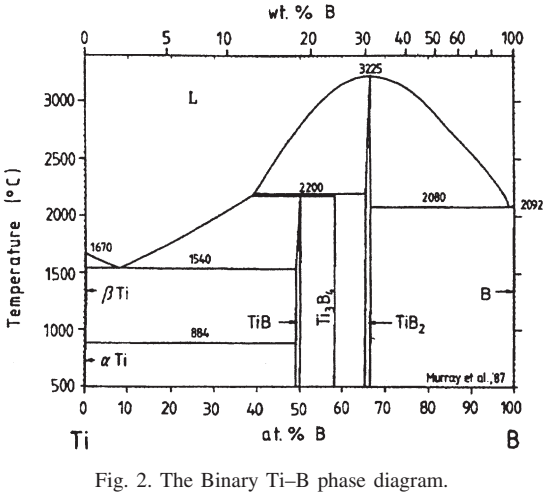

Fig. 2. The Binary Ti–B phase diagram.

densification of the mixed powder and the growth of TiB_2 grains as further discussed in the following.

3.2. Microstructure

Microstructural morphologies of polished surfaces of the sintered specimens are shown in Fig. 3. The 4.8Ti–B_4C material achieved near-full density by hot pressing at 1800°C, Fig. 3(b), whereas about 6% and 3% porosities were found in the 4.8Ti–B_4C hot pressed at 1700°C and the 3Ti–B_4C sample hot pressed at 1800°C, Fig. 3(a) and (c), respectively. This indicates that relative density increased with increasing sintering temperature and with Ti content. Such high relative densities are impossible to attain for the fabrication from the mixture of TiB_2 and TiC powders at a sintering temperature below 2000°C, by just relying on a solid sintering mechanism. It is likely that a much higher local temperature was involved during the reaction sintering due to the reaction heat, which led to a transient liquid sintering mechanism to enhance the densification.

SEM photographs of fractured surfaces of the specimens are shown in Fig. 4. One of the most evident microstructural characteristics is that there are a large number of plate-like grains distributed homogeneously in all these three materials. Figure 5(a) and (b) are the EDAX results of the phases. The plate-like phase is shown to contain Ti, B, and a small level of C, which is most likely to be TiB_2 with C in solid-solution, as further confirmed by the XRD result. In fact, as reported in [18], TiB_2 is of a C32 structure (hexagonal, $a = 3.033$ and $c = 3.23$), constructed by the alternate stacking of Ti planes and the graphite-like B network along the c-direction. The fastest-growing planes of TiB_2 are the $\{1\ 1\ \bar{2}\ 0\}$families with a low-activation energy diffusion path along $< 1\ \bar{1}\ 0\ 0>$ direction, which form a two-dimensional network. Hence TiB_2 tends to grow into a plate-like morphology, with the c-axis perpendicular to the plate plane. The relatively high reaction temperature in the present case largely facilitated the diffusion of B (and Ti) along the low-activation energy diffusion path, and hence the formation of well-developed TiB_2 platelets.

The other phase that forms the matrix is thus TiC_x, as indicated by the XRD result. Among these specimens, the TiB_2 plate-like grains are well developed in the 1800°C hot pressed 4.8Ti–B_4C material, whereas the plate-like morphology is not so evident in the other two materials. Hence, the plate-like morphology of the TiB_2 grains may also be associated with the fact that there is a large quantity of transient liquid phase during sintering of the 4.8Ti–B_4C material at 1800°C, because of both a higher temperature and a higher level of Ti content. The transient liquid resulted from the high temperature seems to facilitate the growth of the TiB_2 crystal.

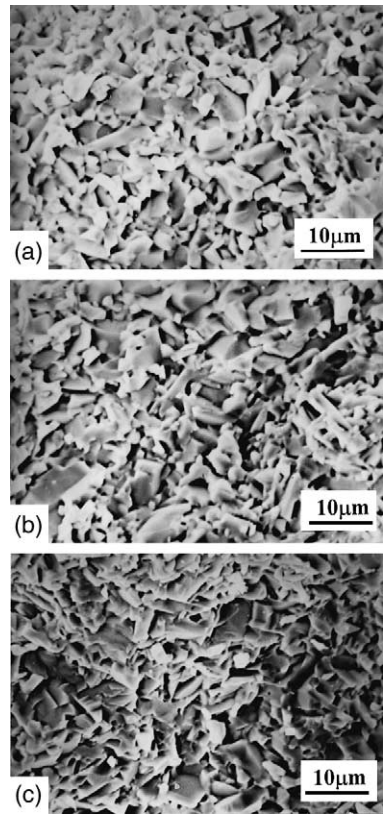

Fig. 4. Photographs showing the fracture surface morphologies of the materials: (a) 4.8Ti–B_4C hot pressed at 1700°C; (b) 4.8Ti–B_4C hot pressed at 1800°C; (c) 3Ti–B_4C hot pressed at 1800°C.

The other reaction product, TiC_x ($x<1$), was located between the TiB_2 grains. It is known that TiC_x, with $x<1$, possesses good plasticity at high temperatures (over the range of 1000–1500°C) [11].

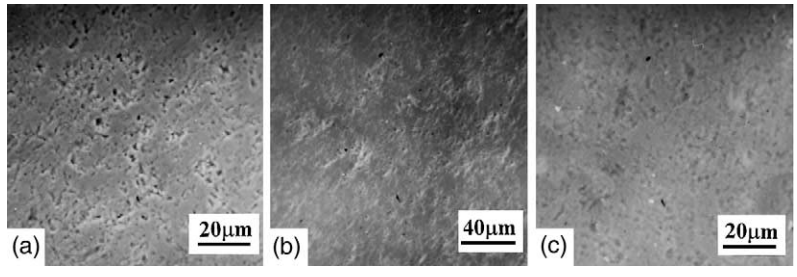

Fig. 3. Photographs showing polished surface morphologies of the materials (a) 4.8Ti–B_4C hot pressed at 1700°C; (b) 4.8Ti–B_4C hot pressed at 1800°C; (c) 3Ti–B_4C hot pressed at 1800°C.

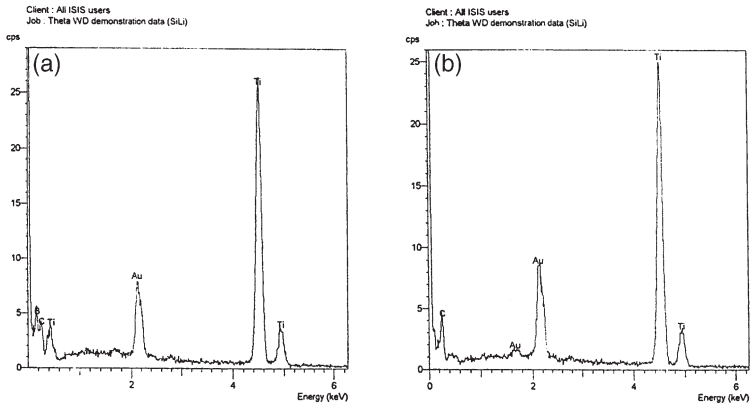

Fig. 5. Typical EDAX results of the plate-like grain (a) and the equiaxial grain (b).

The plastic flow of the TiC_x grains is very beneficial to densification. It can be seen that TiC_x content (and x value) directly affected the process of densification by comparison of the 4.8Ti–B_4C and the 3Ti–B_4C samples, hot pressed at the same temperature (1800°C). The latter has a lower relative density because of its lower TiC_x content and a higher x value [see equations (3) and (5)].

The microstructure is generally uniform in terms of the size, orientation and distribution of the grains, Fig. 6(a), except for a very few abnormally large TiB_2 grains, Fig. 6(b). The TiB_2 platelets are not as regular as the ZrB_2 platelets in the (ZrB_2+ZrC_x) composite produced by the direct reaction of zirconium with boron carbide [13–15]. This is because the present reaction proceeded under pressure, which led to further interruption to the growth of the TiB_2 grains. Nevertheless, the number and size of the plate-like grains in this study are considerably greater than those in the Titanium–Boron–Carbon composites fabricated by hot pressing at 1600°C from the 4Ti–B_4C composition in Ref.[11]. In the latter case, the plate-like grains were determined as Ti_3B_4. The differences in the morphologies of the plate-like grains and in the relative densities of the materials are largely responsible for the variation in the mechanical properties of the materials (see Section 3.3).

Further microstructural analysis was carried out by TEM for the 4.8Ti–B_4C material hot pressed at 1800°C. Figure 7 shows the TEM images of the grain structures. The plate-like TiB_2 grains are evidently observed. The thickness of the plate is uniform and is about 0.5–2 μm. The shape and dimensions of the

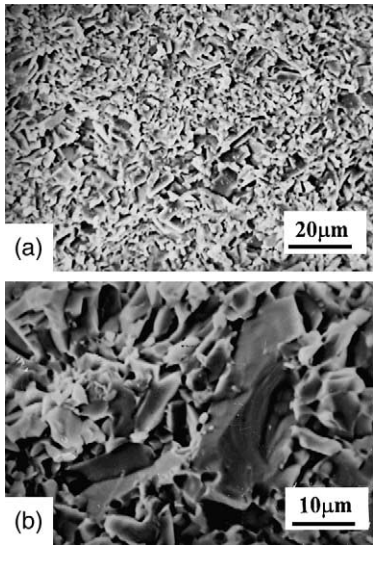

Fig. 6. Morphology of the fractured surface of the 4.8Ti–B_4C sample hot pressed at 1800°C, showing the grain structure and distribution (a), and the abnormal grain growth of TiB_2 (b).

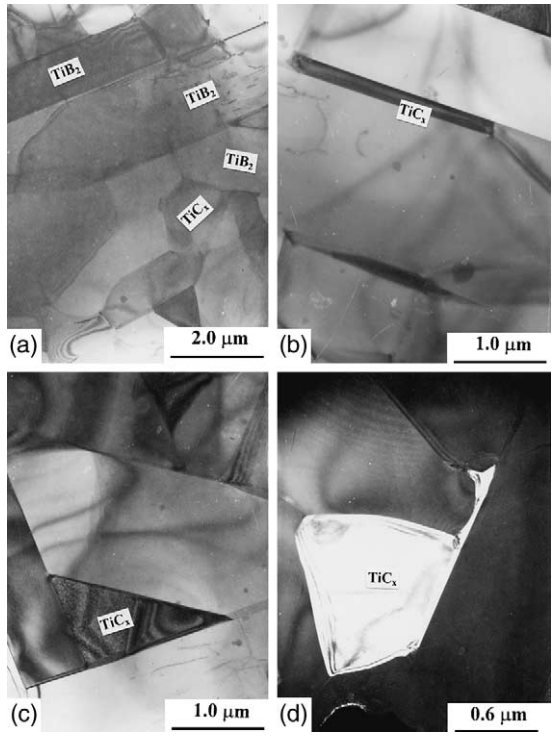

Fig. 7. TEM photographs showing grain distributions of the 4.8Ti–B_4C sample hot pressed at 1800°C: (a) overall distribution of the grains; (b) a plate-like TiC_x grain; (c) a triangular TiC_x; and (d) an irregular TiC_x (dark field image).

planar plane cannot be accurately determined at this stage, but seem to be dependant on the growth of the other grains in its vicinity. For example, most of the TiB_2 grains possess regular platelet morphologies with straight edges, but some are with irregular shape and curved edges. However, TiC_x grains have no specific morphology, its shape was completely defined by the surrounding grains. For example, a plate-like TiC_x is located between two parallel TiB_2 grains [see Fig. 7(b)], a triangular TiC_x is in the corner of three interwoven TiB_2 grains [see Fig. 7(c)], and an irregular shaped TiC_x is surrounded by a number of grains (including other TiC_x grains) [Fig. 7(d)]. From these distribution patterns, it seems that the TiB_2 plate-like grains were formed prior to the TiC_x grains. The formation of the TiC_x grains proceeded at the same pace as the densification of the materials. Hence TiC_x is likely to be the "matrix" of the composite.

In most of the TiB_2 grains, many inclusions and defects were identified, such as cavities, free carbon, and dislocations, as shown in Fig. 8. The cavities were likely to be the result of the entrapped gases related to the rapid growth of TiB_2 grains and to volume change during phase transformation. Carbon inclusions exist at two types of locations and in two forms. One is within the TiB_2 grains in the form of carbon clusters, as also indicated by the EDAX results in Fig. 5(a), showing the existence of carbon. Another is in the boundaries of the grains in the form of nearly amorphous carbon particles [as indicated in the inset of the diffraction pattern in Fig. 8(a)]. Whether the free carbon was from the B_4C powder or the graphite die or both is unclear at present. The fact that no free titanium was found by XRD and EDAX may lend proof that the vaporisation of carbon from the graphite die and its diffusion into the reaction products contribute to the excess carbon.

Dislocations are not only present within the TiB_2 grains but are also observed within a TiC_x grain close to the TiC_x/TiB_2 interface, as shown in Fig. 9. The dislocation pile-up in the TiC_x grain in front of the interface implies the occurrence of some plastic-deformation of the TiC_x phase during processing.

3.3. Properties

The results of the mechanical properties are listed in Table 1. Higher flexural strengths of 453–680 MPa and excellent fracture toughness of 8.4–12.2 $MPa\bullet m^{1/2}$ were obtained for these three composites. The variation in the mechanical properties is well reflected in the change in microstructural features. The 4.8Ti–B_4C material hot pressed at 1800°C, with the highest relative density and sufficiently grown TiB_2 plate-like grains, possesses the highest flexural strength and fracture toughness. Whereas the 3Ti–B_4C material hot pressed at 1800°C, with the lowest relative density and an insufficient amount of TiB_2 plate-like grains, exhibits the lowest flexural strength and fracture toughness. However, the strength and toughness of the latter are still much higher than those of the 3Ti–B_4C material (hot pressed at 1600°C) reported by Barsoum and Houng [11]. These are also much higher than those of the 1000°C processed 3Ti–B_4C material in [12]. Furthermore, it is noted that both a relatively high strength of 680 MPa and an extremely high toughness K_{IC} of 12.2 $MPa\bullet m^{1/2}$ were achieved for the 4.8Ti–B_4C material hot pressed at 1800°C. In comparison, a strength of 590 MPa and a toughness of 5.6 $MPa\bullet m^{1/2}$ were obtained in Barsoum and Houng's work for a 4Ti–B_4C material hot pressed at 1600°C, even with a high relative density of 99.9%. Clearly, the *in situ* toughening effect has been much

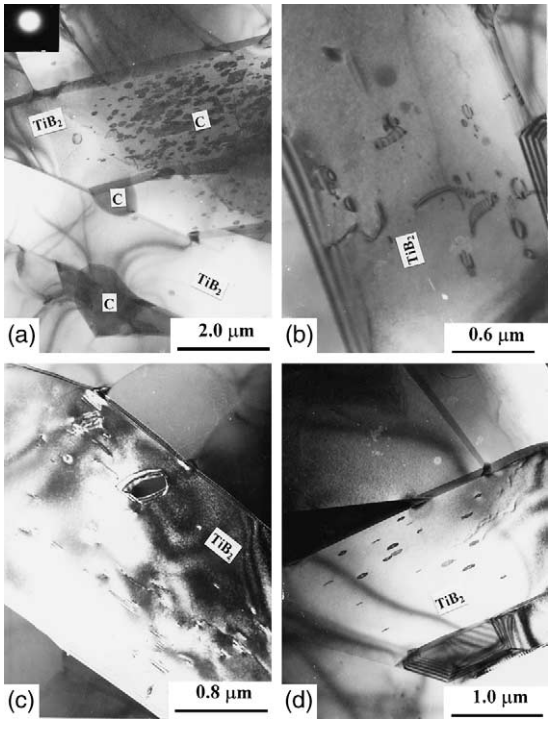

Fig. 8. TEM photographs showing impurities and defects in the 4.8Ti–B_4C sample hot pressed at 1800°C: (a) carbon inclusion (inset showing the SAD pattern of interfacial carbon); (b)–(d) showing unknown inclusions or defects.

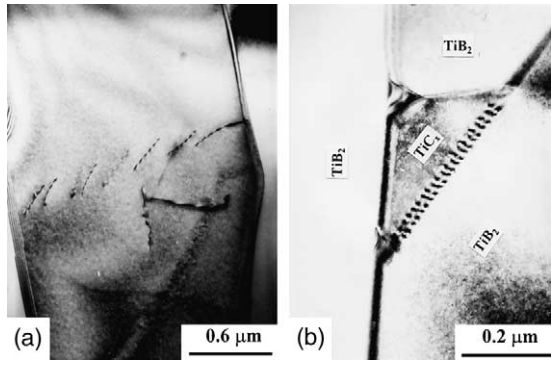

Fig. 9. TEM photographs showing dislocations in the 4.8Ti–B_4C sample hot pressed at 1800°C: (a) dislocations within a TiB_2 grain; and (b) dislocation activity during deformation of TiC_x at an TiB_2/TiC_x interface.

enhanced by the occurrence of the well-developed TiB_2 plate-like grains in the present case, which is associated with a relatively high sintering temperature and a relatively high Ti content.

A number of (TiB_2+TiC+SiC) composites have been processed by Mestral and Thevenot [7] using hot pressing from a mixture of TiB_2, TiC and SiC powders. Since the grain growth was inhibited by this method, the resultant materials usually possess a high strength. A maximum bending strength of 1100 MPa was obtained in a (TiB_2+TiC) system with a small SiC content. However, because it involved solid-state sintering mechanisms, the TiB_2 plate-like grains were not formed, and hence the toughening effect was very limited. The K_{IC} was measured to be only 5.2 $MPa\bullet m^{1/2}$. Thus, it is vital for TiB_2 to exist as well-developed plate-like grains in order to achieve highly toughened TiB_2–TiC composites.

The typical fracture surface of the 4.8Ti–B_4C material hot pressed at 1800°C is shown in Fig. 10 [Here the TiB_2 platelets are slightly larger than those shown in Fig. 4(a), due to sampling at different positions of the specimen where different local temperatures may have led to variations in the platelet size]. Evidence of both intergranular and transgranular fracture behaviours is present. Both the equiaxial TiC_x grains and the smaller TiB_2 plate-like grains fractured mainly in an intergranular manner. The relatively thick TiB_2 grains fractured predominantly by the transgranular mode. Some degree of pull-out of the platelets can also be noted. In the latter case, it seems that the crack initiated at the interface from one side of a TiB_2 grain, and propagated along and around this interface and then appeared on the opposite side of the TiB_2 grain for a short distance, forming a zigzag crack propagation path. Such a tortuous crack path resulted in a rough fracture surface and enhanced the toughness.

The intergranular fracture is likely to be the result of a weak interfacial bonding or a strong interfacial strain field, which is related to the mismatch of the thermal expansion coefficients (CTE) between the grains. The thermal expansion of the TiB_2 grain is anisotropic with $\alpha_c = 9.77\times10^{-6}$ K^{-1} and $\alpha_a = 7.19\times10^{-6}$ K^{-1} [19], whereas that of TiC is isotropic with $\alpha = 7.20\times10^{-6}$ K^{-1}. The CTE of TiB_2 along the c-axis is greater than that of TiC, and the CTE of TiB_2 along the a-axis is almost the same as that of TiC. As discussed in Section 3.2, the c-axis of the TiB_2 platelet is perpendicular to the platelet plane and the a-axis is parallel to the platelet plane, as further illustrated in Fig. 11. Therefore, at the interface perpendicular to the c-axis of the TiB_2 platelet, Interface I, there exist a very weak shear stress and a strong normal tensile stress in the TiB_2 grain, leading to weak interfacial bonding. At the interface parallel to the c-axis of TiB_2 grain, Interface II, the stresses are a small normal tensile stress and a large shear stress (tensile on the TiB_2 side and compressive on the TiC_x side). It is the interfacial stress that "attracts" cracks, rendering the cracks propagate tortuously along the interfaces, and therefore consume more fracture energy and produce toughening effects, i.e. stress field toughening. The effect of stress field toughening is enhanced by the presence of the well-developed TiB_2 grains because the increment of fracture toughness (ΔK_{IC}) resulted from such a mechanism increases with the local residual compressive stress in the TiC_x matrix, and with the volume fraction and the equivalent diameter of reinforcement TiB_2, respectively.

Since the interfacial shear stresses on the side of TiC_x are compressive at both Interfaces I and II, the TiC_x matrix was protected and no transgranular fracture could occur in the TiC_x grains. On the other hand, although a tensile stress existed on the TiB_2 side at Interface II, it could not result in crack propagation across the TiB_2 grain in the direction parallel to the c-axis of TiB_2, because of its very small thickness. Hence, when the crack tip encounters the TiB_2 grains, it either bypasses the TiB_2 grain (leading to pull-out of the TiB_2 grain) or propagates across it in a zigzag manner (leading to fracture of the TiB_2 grains), depending on the specific position of the crack, as indicated in Fig. 11. Therefore the main toughening mechanisms include stress field toughening, crack deflection, and the pull-out and fracture of the TiB_2 plate-like grains. All of these mechanisms contributed to the exceptionally high toughness, as well as good strength, in the present composites.

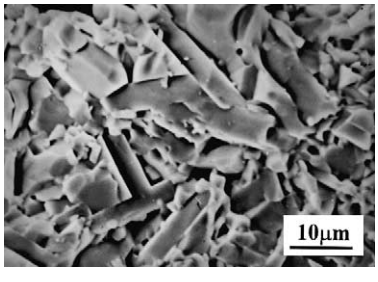

Fig. 10. SEM photograph showing fracture feature of the 4.8Ti–B_4C sample hot pressed at 1800°C.

4. CONCLUSIONS

Tough TiB_2–TiC composites have been successfully synthesised by means of *in situ* reaction of B_4C and Ti powder mixtures at relatively high temperatures. Powder mixtures of Ti:B_4C molar ratios of

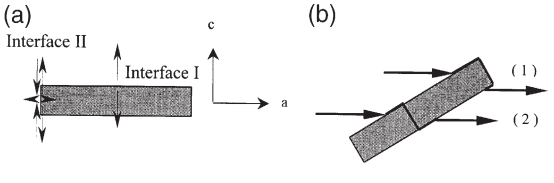

Fig. 11. Schematic diagrams showing: (a) the interfacial stress states around the plate-like TiB_2 grain; and (b) the crack paths of around (1) and across (2) the plate-like TiB_2 grain.

3:1(3Ti–B_4C) and 4.8:1(4.8Ti–B_4C) were completely transformed to high density (TiB_2+TiC_x) composites, when hot pressed at 1700°C ~1800°C under 35 MPa for 60 min. No Ti_3B_4, TiB, Ti_2B_5 and free Ti phases were identified in the samples by XRD and EDAX analyses.

The high sintering temperature is believed to be the key to achieving the high relative density and the well-developed plate-like morphology of the TiB_2 grains. As a result, the reaction, densification and grain growth proceeded by a transient liquid mechanism. The transformation of Ti_3B_4 into TiB_2, and the flow and/or vaporisation of Ti and the graphite die also occurred in the local high-temperature environment. The rapid growth of the TiB_2 grains led to many inclusions and defects within the TiB_2 grains.

Rather high fracture toughness (K_{IC} up to 12.2 MPa•$m^{1/2}$) has been obtained here by the simple hot pressing of the mixture of Ti and B_4C powders. This is attributed to the high relative density and the existence of well-developed TiB_2 plate-like grains. The main toughening mechanisms include crack deflection and the pull-out and fracture of the TiB_2 plate-like grains.

Acknowledgements—The project was kindly supported by The Chinese Postdoctoral Funding Committee (awarded to GW), and partly by The Royal Society (UK) under the FCO Chevening Fellowship scheme.

REFERENCES

1. Telle, R. and Petzow, G., *Mater. Sci. Eng. A*, 1988, **105–106**, 97.
2. Williams, W. S., *J. Appl. Phys.*, 1964, **35**, 1329.
3. Ramberg, J., Wolfe, C. and Williams, W., *J. Am. Ceram. Soc.*, 1985, **68**, C78.
4. Kim, D. K. and Kim, C. H., *Adv. Ceram. Mater.*, 1988, **3**(1), 52.
5. Kang, E. S. and Kim, C. H., *J. Mater. Sci.*, 1990, **25**, 580.
6. Sigl, L. S. and Schwetz, K. A., *Jpn. J. Appl. Phys.*, 1994, **10**, 224.
7. de Mestrel, F. and Thevenot, F., *J. Mater. Sci.*, 1991, **26**, 5547.
8. Moriyama, M. and Aoki, H., *J. Ceram. Soc. Jpn, Int. Ed.*, 1997, **104**, 320.
9. Sasaki, S., Suga, T., Yanai, T., Suganuma, K. and Niihara, K., *J. Ceram. Soc. Jpn, Int. Ed.*, 1994, **102**, 320.
10. Hofmann, H. and Petzow, G., *J. Less-Common Met.*, 1986, **117**, 121.
11. Barsoum, M. W. and Houng, B., *J. Am. Ceram. Soc.*, 1993, **76**(6), 1445.
12. Gotman, I., Travitzky, N. A. and Gutmanas, E. Y., *Mater. Sci. Eng.*, 1998, **A244**, 127.
13. Johnson, W. B., Claar, T. D. and Schiroky, G. H., *Ceram. Eng. Sci. Proc.*, 1989, **10**(7–8), 588.
14. Claar, T. D., Johnson, W. B., Anderson, C. A. and Schiroky, G. H., *Ceram. Eng. Sci. Proc.*, 1989, **10**(7–8), 599.
15. Johnson, W. B., Nagelberg, A. S. and Breval, E., *J. Am. Ceram. Soc.*, 1991, **74**(9), 2093.
16. Brodkin, D. and Barsoum, M. W., *J. Am. Ceram. Soc.*, 1996, **79**(3), 785.
17. Murray, J. L., Liao, P. K. and Spear, K. E., *Bull. Alloy Phase Diag.*, 1986, 7550.
18. Fan, Z., Guo, Z. X. and Cantor, B., *Compos. Part A*, 1997, **28**, 131.
19. Ferber, M. K., Becher, P. F. and Finch, C. B., *J. Am. Ceram. Soc.*, 1993, **76**(1), C2.